

Ultrathin epitaxial iron films on a highly asymmetrical substrate: Fe/Cu(311)

S. Fölsch, B.-Ch. Choi, and K. H. Rieder

Institut für Experimentalphysik, Freie Universität Berlin, Arnimallee 14, 14195 Berlin, Germany

(Received 17 June 1996)

The structure and morphology of ultrathin epitaxial Fe films on Cu(311) is examined *in situ* by spot-profile analyzing low-energy electron diffraction. Cu(311) is a highly asymmetrical substrate which is characterized by a troughlike surface structure composed of uniaxially arranged close-packed Cu atom rows. Deposition at 140 K initially leads to the formation of pseudomorphic Fe. The constraint to lower dominant stress along the close-packed atom rows forces the formation of pseudomorphic patches with a quasiperiodic separation of 35 Å. With proceeding growth, these patches act as nucleation sites for three-dimensional islands that gradually relax via a Pitsch transformation towards a strained bcc structure. Coalescence occurs at ~ 5 ML and leads to a periodically faceted growth front of the overlayer. The resulting surface topography corresponds to a regular up-and-down staircase and remains unchanged for coverages >5 ML: the periodic facet separation measures 35 Å; 7–8 layers contribute to the growth front. As a consequence of coalescence, the film locks into a lattice arrangement which is predominantly dictated by the substrate and is likely to correspond to an fcc-like structure. The periodic faceting of the film surface, on the other hand, allows partial relaxation towards strained bcc structure to persist in the top layers of the film. [S0163-1829(96)07340-7]

I. INTRODUCTION

The heteroepitaxial growth of metal films on single-crystal substrates opens up the possibility of producing crystallographic phases that are not stable in bulk material. A prominent example for a material fabricated in this way is the thin-film-system Fe/Cu(100).^{1–10} The Cu host stabilizes the formation of fcc Fe (γ -Fe), which exists only at elevated temperatures in the bulk (>1180 K). γ -Fe is especially attractive because it supports ferromagnetic, antiferromagnetic, and nonmagnetic order, depending on the lattice constant.¹¹ As a consequence, the magnetic state of γ -Fe films can be varied in a controlled manner by choosing appropriate growth parameters.¹² Beyond this aspect, magnetic properties become extremely structure sensitive in ultrathin films. For instance, significant influences of the film morphology (i.e., step densities, island sizes) on Curie temperature and magnetic moments¹³ and a decisive role of epitaxial strain on preferred magnetization directions¹⁴ have been observed.

The present study aims at the growth and characterization of ultrathin Fe films showing an anisotropic morphology. A spatial anisotropy of the film topography is expected to have considerable influence on the magnetic film properties. To achieve this we have chosen a Cu(311) template that provides a highly asymmetrical surface structure composed of uniaxially arranged close-packed atom rows. This enables quasi-one-dimensional migration of adatoms¹⁵ on the Cu(311) surface. It is further expected that the pronounced asymmetry of the substrate surface may cause uniaxial stress in the deposited overlayer. We will show that the relief of uniaxial stress is indeed the driving force that produces a film topography of spatial anisotropy in the present case. Conversely, the morphology has dominant impact on the relief of lattice distortions and on the crystal structure of the film.

II. EXPERIMENT

The investigations were performed in a UHV system providing a base pressure of $<1 \times 10^{-8}$ Pa. A chemomechanical polished Cu(311) crystal surface (purchased from Fa. Mateck) was cleaned by alternate Ne⁺ sputtering (800 eV, ion current $\sim 1 \mu\text{A}$) and annealing at 800 K. After repeated preparation cycles, no residual contamination was detectable by x-ray photoelectron spectroscopy (XPS). A low-energy electron-diffraction (LEED) pattern showing bright and sharp spots proved that this cleaning procedure leads to a smooth and well ordered substrate surface with a defect-free length of typically ~ 300 Å. The specimen could be cooled by liquid nitrogen. The sample temperature was measured by a NiCr/Ni thermocouple. Fe was deposited from an electron-beam evaporator at a rate of ~ 0.5 Å/min. Coverages were estimated by monitoring XP signals from the Cu substrate and the Fe overlayer. The films grown were investigated *in situ* by Spot-Profile Analyzing LEED (SPALEED),¹⁶ which provides detailed quantitative information on the surface morphology and its defect structure.¹⁷

III. RESULTS AND DISCUSSION

The hard-sphere model in Fig. 1 illustrates the structure of the Cu(311) surface; it is composed of close-packed Cu atom rows along the $[01\bar{1}]$ direction with a nearest-neighbor distance of 2.55 Å and a row separation of 4.23 Å. The uniaxial arrangement of Cu atom rows causes a troughlike surface structure with a centered rectangular Bravais lattice (i.e., a parallelogram-shaped primitive unit mesh).

Deposition of ~ 1 monolayer (ML) Fe at 140 K leads to the LEED pattern shown in Fig. 2. A low substrate temperature was chosen to avoid possible intermixing¹⁸ at the interface. At this stage, no extra spots are observed. This indi-

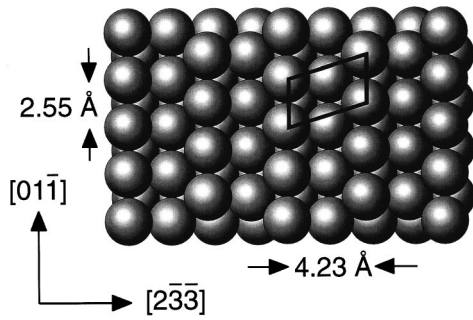


FIG. 1. Hard-sphere model of the Cu(311) substrate surface with a parallelogram-shaped primitive unit mesh.

icates that a pseudomorphic Fe overlayer is formed in the initial stage, which is characteristic of ultrathin Fe films grown on Cu substrates.^{1–10} Additional features are present in the diffraction pattern: close to the integral order spots, discrete intensity shoulders occur along the $[01\bar{1}]$ direction (i.e., the direction of close-packed rows). These features do not originate from an undulated incommensurate overlayer¹⁹ or a surface reconstruction due to buckled atom rows as observed for fcc Fe (γ -Fe) films on Cu(100).^{6,10} Instead, the shoulders reflect the vertical roughness of the surface, as is evident from their characteristic energy-dependent intensity variation. For a given integral order spot, the shoulders vanish when the kinetic energy of incident electrons is adjusted to an in-phase scattering condition [i.e., integral numbers of the vertical scattering phase $S = |\mathbf{K}_\perp|d/(2\pi)$, where d de-

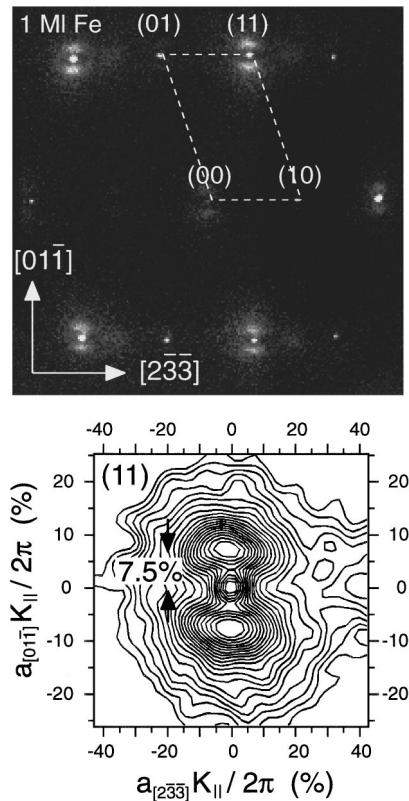


FIG. 2. LEED pattern after deposition of 1 ML Fe at 140 K showing integral-order spots with peaked intensity shoulders along the close-packed-row direction (upper panel) and contour plot of the (11) spot at a vertical phase of $S = 1.9$ (lower panel).

notes interlayer spacing]. Hence, the diffuse intensity is predominantly determined by the geometrical phase shift $|\mathbf{K}_\perp|d$ between electron waves scattered at adjacent terraces of the rough surface. As is apparent from the sharply peaked appearance of the diffuse intensity, the Fe overlayer is characterized by an additional quasiperiodic correlation along close-packed rows with a periodicity length of 35 Å [corresponding to a shoulder distance of 7.5% of the surface Brillouin zone (SBZ); 100% relates to the reciprocal nearest-neighbor distance within a row]. The long-range correlation as indicated by the shoulder separation proves to be independent of coverage in the submonolayer regime. This behavior suggests that pseudomorphic three-dimensional (3D) γ -Fe islands build up at a net coverage of ~ 1 ML that are characterized by a fixed quasiperiodic separation along the close-packed-row direction. We propose that this long-range-ordered island arrangement originates from anisotropic lateral stress imposed by the substrate. Assuming a cubic-lattice constant of $a_0 = 3.57$ Å (as extrapolated from the high-temperature equilibrium phase of γ -Fe) the pseudomorphic γ -Fe overlayer is strained by +1.2% both parallel and perpendicular to atom rows. This pseudomorphic strain will lead to dominant uniaxial stress along the close-packed-atom rows. Consequently, the growth of a compact pseudomorphic layer along this direction is energetically unfavorable. Instead, it will be more favorable to create small islands to relieve strain. Such an instability against shape changes is a characteristic feature of films under stress.²⁰ The observed periodicity of pseudomorphic Fe islands along the row direction is a further consequence of their strained state: it has been shown both theoretically^{21–23} and experimentally^{24–26} that elastic strain relief promotes the formation of long-range-ordered arrangements via effective long-range repulsion between strained islands.

For coverages > 1 ML, a highly distorted Fe overlayer is formed. With increasing coverage, the observed crystallographic structure proceeds to a strained bcc-like arrangement. Figure 3 shows a related diffraction pattern obtained after deposition of 5 ML Fe which exhibits a rectangular unit mesh. Pattern symmetry and size of the reciprocal-lattice constants indicate a bcc Fe(211) orientation. Figure 4 illustrates a hard-sphere model of the Fe(211) surface: again, the surface is composed of parallel close-packed-atom rows with a nearest-neighbor distance and a row separation close to that of the Cu(311) substrate. However, in this case the arrangement of adjacent rows is described by a primitive rectangular unit mesh. Close-packed-atom rows of the Fe films are aligned parallel to those of the Cu substrate. The orientational relationship observed here resembles characteristic features of Fe films on Cu(100), where the transition from pseudomorphic fcc Fe to the intrinsic bcc structure is ruled by a Pitsch transformation.^{8,10} This transformation preserves the close-packed rows of nearest-neighbor atoms, i.e., face diagonals of the fcc lattice convert to bcc body diagonals. The rearrangement is realized via a shear distortion along the row direction combined with compressions and expansions of the lattice. In the present case, we can directly follow the coverage-dependent evolution of these lattice distortions, which will be discussed in detail below.

At this point, it is instructive to focus on the morphological features. The spot broadening deduced from the LEED

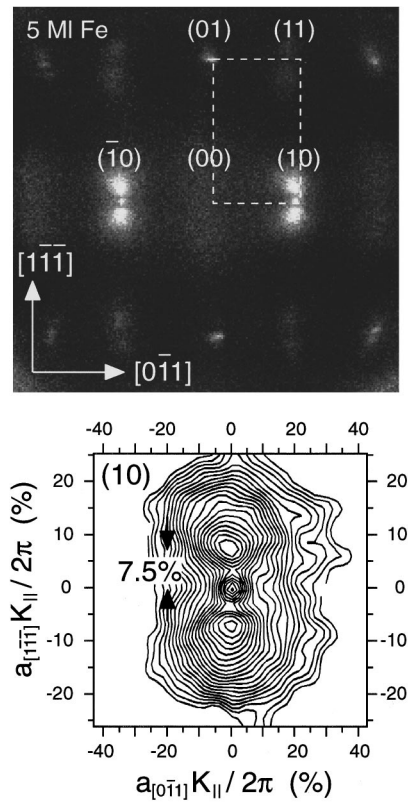


FIG. 3. LEED pattern of a 5-ML-thick bcc Fe(211) overlayer grown at 140 K showing diffuse intensity shoulders along the close-packed-row direction (upper panel) and contour plot of the (10) spot at a vertical phase of $S = 1.9$ (lower panel).

pattern in Fig. 3 indicates significant roughness of the strained bcc Fe overgrowth. A slight deviation from the in-phase scattering condition produces pronounced diffuse intensity which, again, is composed of peaked shoulders along the close-packed-row direction. At this stage, however, the shoulders shift continuously toward the central spike when the vertical scattering phase is changed from a noninteger value toward the Bragg condition. Eventually, the shift staginates at a minimal shoulder distance of 7.5% SBZ close to the Bragg condition. This is illustrated in the upper panel of Fig. 5, where a set of (00) spot profiles is shown that was obtained for a 9-ML-thick overlayer. The lower panel shows the phase-dependent shift of the shoulder positions in detail. First, we address the regime in which the shoulder positions vary linearly with the scattering phase. This behavior is char-

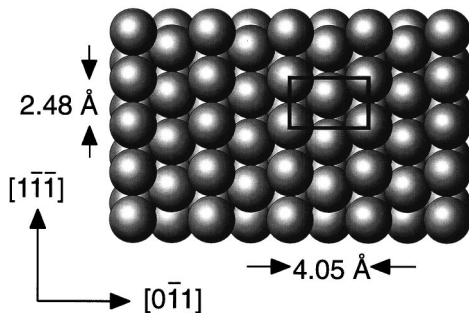


FIG. 4. Hard-sphere model of the bcc Fe(211) surface with a rectangular primitive unit mesh.

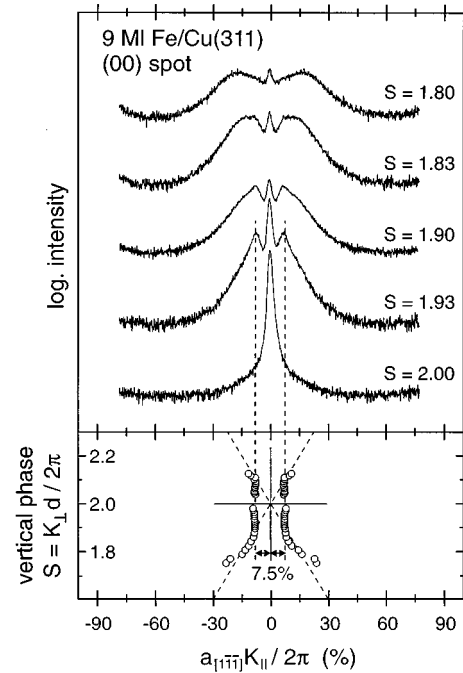


FIG. 5. (00) spot profiles obtained for a 9-ML-thick Fe overlayer along the row direction at different vertical phases S (upper panel) and phase-dependent positions of the peaked intensity shoulders (lower panel).

acteristic for a periodically faceted surface with a regular up-and-down staircase and has been observed for various epitaxial metal-on-metal systems.²⁷⁻²⁹ The phase-dependent shoulder shift that results from such a surface topography is visualized with the help of the Ewald construction: the shoulder positions are determined by facet rods inclined with respect to the (00) rod. In the present situation, a mean facet normal inclination of 24° with respect to the $[211]$ direction is determined. This angle is in the range of inclinations expected for low-index facets with a $[111]$ orientation (19.5° inclination) or a $[100]$ orientation (35.3° inclination). However, particular contributions to the shoulder profiles in Fig. 5 are not resolved; they appear to be considerably broadened. This may be due to a certain degree of orientational disorder and the finite size of facets present. The stagnation of the shoulder positions at a minimal distance of 7.5% SBZ (which equals the stationary shoulder position found for the pseudomorphic overlayer) is a further consequence of the finite facet size. According to general ideas of diffraction theory, the smallest scattering vector caused by a periodic array corresponds to the largest spatial correlation present. Consequently, the minimal shoulder distance of 7.5% SBZ (i.e., the smallest scattering vector $K_{||}$ possible) is identified with the periodicity of the up-and-down staircase of the faceted surface. A similar finite-size effect in the diffraction of a faceted surface has been observed previously for the heteroepitaxial system Ge/Si(001).³⁰ The periodicity of the regular facet array is well confined to 35 Å, as is evident from the sharply peaked shoulder profile close to the Bragg condition. It proves to be constant over the entire coverage range investigated, that is, for coverages of 1–20 ML. Apparently, the characteristic periodicity length of the facet array is determined by the quasiperiodic separation of pseudo-

morphic patches formed in the initial stage. This suggests that the growth process is characterized by the formation of 3D islands that nucleate on top of the pseudomorphic seed layer and convert into a periodic array of strained bcc islands by means of a Pitsch transformation. This transformation is accompanied by a considerable shear, i.e., a dislocation of close-packed-atom rows along the row direction. Consequently, effective strain relief is expected to occur along the rows. This is indeed observed and will be discussed in detail below.

Apart from the lateral roughness contained in the spot profile $I(S, K_{\parallel})$, as shown in Fig. 5, the energy dependence of the relative central spike intensity $I(S, K_{\parallel}=0)/I_{\text{total}}$ gives information on the vertical layer distribution.¹⁷ The normalization of $I(S, K_{\parallel}=0)$ to the total spot intensity eliminates the energy-dependent form factor and thus provides the kinematic structure factor $G(S)$ as a suitable measure for the vertical surface roughness.³¹ The precondition necessary for the separability into a dynamic form factor and a kinematic structure factor is fulfilled within the framework of the kinematic approximation,³² which assumes identical form factors for all scattering units. In this case, the phase shift between electron waves scattered at a rough surface is determined by the geometrical phase shift only. This leads to a variation of the kinematic structure factor $G(S)$ which is symmetrical with respect to the in-phase scattering condition where the phase shift equals 2π . The full width at half maximum of the $G(S)$ curve yields the asperity height Δ , i.e., the root-mean-square (rms) value of the vertical roughness.¹⁷ If scattering units with different dynamic form factors (e.g., different species of atoms) are present at the surface, an additional contribution to the phase shift is given by the different energy dependence of particular form factors. This produces a variation of the relative central spike intensity which, in general, is more complicated.³³ As a consequence for the present case, strictly quantitative information on the vertical roughness is only deducible when the Fe overlayer is completely coalesced. Indeed, the assumption that $G(S)$ is given by the normalized spike intensity $I(S, K_{\parallel}=0)/I_{\text{total}}$ is based on a further approximation. It implies that the form factor $F(\mathbf{k}_i, \mathbf{k}_j)$ is essentially constant over the range of scattering vectors \mathbf{K}_{\parallel} for which the spot profile is evaluated. The majority of investigated cases shows that this condition is fulfilled fairly well, i.e., the form factor varies sufficiently slowly³⁴ with \mathbf{K}_{\parallel} . Our data suggest that this requirement is met also in the present case: the design of the SPAL-LEED system¹⁶ leads to a scattering geometry in which the incident electron beam direction (i.e., the direction of the incident wave vector \mathbf{k}_i) is 4° or 60° off the surface normal. For both these configurations and at different scattering conditions, we always observed shoulder profiles symmetrical with respect to the central spike. We thus can exclude a significant variation of $F(\mathbf{k}_i, \mathbf{k}_k)$ as a function of \mathbf{k}_i which is asymmetrical with respect to the surface-normal direction. In Fig. 6, the relative intensity variation of the central spike is plotted versus the vertical phase S for coverages above ~ 5 ML. The derived $G(S)$ curve is sharply peaked and fairly symmetrical with respect to the in-phase condition. In contrast, for coverages below 5 ML a considerable deviation from a symmetrical curve shape is observed. This suggests that the Fe overlayer that initially forms separate 3D islands has coalesced at ~ 5

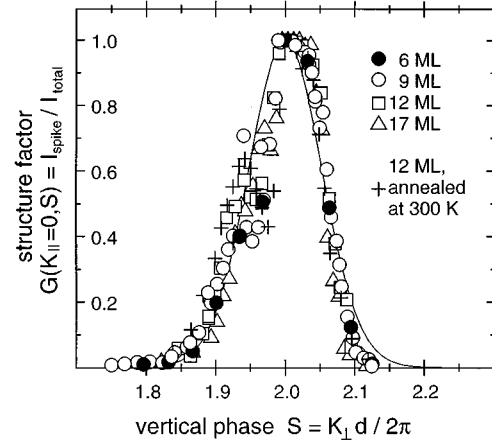


FIG. 6. Kinematic structure factor $G(S)$ as derived from the relative intensity variation of the central spike for different film thicknesses. The rms value of the vertical roughness [deduced from the halfwidth of the $G(S)$ curve] is constant for coverages >5 ML and measures $2\text{--}2.2 \text{ \AA}$ (i.e., 7–8 layers contribute to the growth front). Full line corresponds to a calculated curve for statistical layer distribution; the vertical roughness is not affected by subsequent annealing at 300 K (as denoted by crosses).

ML. Hence, an evaluation based on the kinematic approximation is valid for the data plotted in Fig. 6. The peaked curve shape reflects constructive scattering between adjacent terraces for integer values of $S = |\mathbf{K}_{\perp}|d/(2\pi)$ and a rapidly decreasing intensity due to destructive scattering when the phase deviates from the in-phase condition. The vertical roughness is constant over the entire coverage range investigated. Consequently, the faceted surface topography remains unchanged after the film has coalesced. An asperity height of $\Delta = 2.0\text{--}2.2 \text{ \AA}$ is deduced from the full width at half maximum, which is equivalent to 7–8 layers contributing to the growth front of the film. The observed completion of coalescence at 5 ML may be verified by a simple estimate: for a model surface structure consisting of strictly periodic ridges with a facet inclination of 24° and a separation of 35 \AA , coalescence is achieved at ~ 4 ML coverage.

In the coverage regime below 5 ML, where the overlayer transforms from pseudomorphic fcc structure to a strained bcc film, the relaxation of the shear distortion is deducible from a careful inspection of the Fe LEED spots. A sequence of line scans along the positions of first-order LEED spots along the $[0\bar{1}1]$ Fe direction (i.e., the direction perpendicular to close-packed rows) is shown in Fig. 7. At a coverage of ~ 2.5 ML, both substrate and Fe spots are present. This gives further evidence of the formation of 3D Fe islands that are not completely coalesced at this stage. The Fe spots are split up along the $[011]$ Fe direction. They appear as a doublet of spots with a separation of $\sim 25\%$ SBZ for the present coverage (100% SBZ relates to the size of the surface Brillouin zone along the $[011]$ Fe direction). Their positions are marked by dashed lines in Fig. 7. The electron energy for which a particular component of each doublet is observed with maximum intensity coincides fairly well with Bragg conditions calculated for related bcc spot orders (i, j) for a (211) orientation as indicated in Fig. 7. In this way, each doublet is identified with a pair of nonequivalent spots with indices $(i, j=1)$ and $(-i, j=-1)$, respectively. This be-

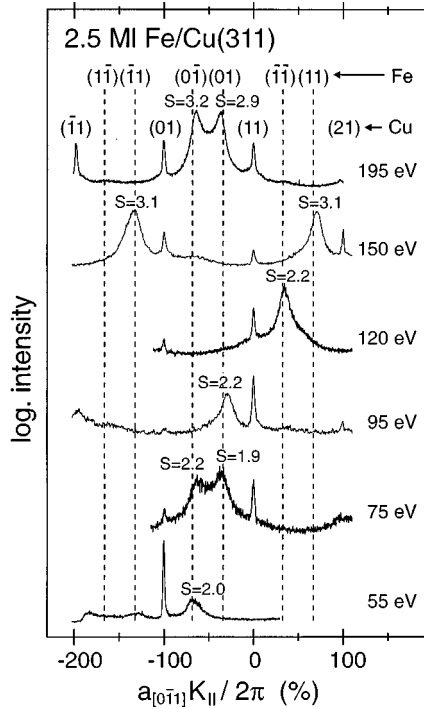


FIG. 7. Sequence of line scans along the positions of first-order LEED spots along the $[0\bar{1}1]$ Fe direction for 2.5-ML coverage. Fe spots are split up in a doublet (positions elucidated by dashed lines); each spot of the doublet shows in-phase energies close to those expected for bcc Fe spots with indices (i,j) as indicated.

havior becomes immediately clear with the help of Fig. 8, where the positions and indices of all observed Fe spots are plotted schematically. The entire spot arrangement is consistent with the formation of rotated twin domains and a uniaxial shear of each twin along the close-packed-row direction. The progression of this lattice shear is manifested by a continuous decrease of the spot splitting with increasing coverage. The upper panel of Fig. 9 shows the coverage-dependent evolution of the shear in detail: the angle between the unit vectors that determine the primitive unit mesh of the distorted film surface is plotted versus coverage. Arrows de-

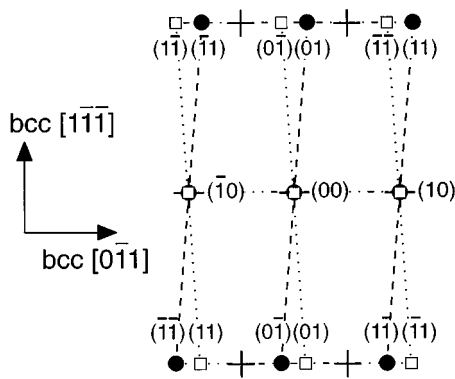


FIG. 8. Scheme of the complete diffraction pattern: crosses denote Cu substrate spot positions, squares and circles correspond to Fe spots with related indices (i,j) . The entire spot arrangement is generated by two twinned bcc Fe(211) domains, each of which is sheared along the close-packed-row direction.

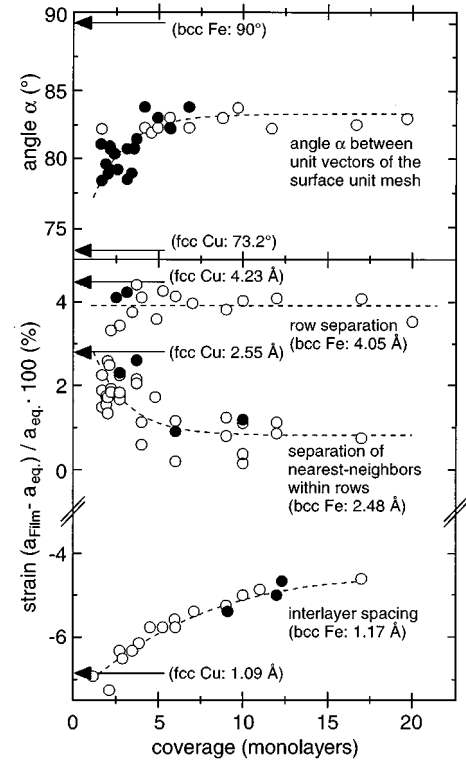


FIG. 9. Coverage-dependent evolution of the lattice parameters of the Fe overlayer: upper panel shows the angle between unit vectors of the surface unit mesh reflecting uniaxial shear along the rows; lower panel illustrates lateral strains [with respect to bcc Fe(211) equilibrium configuration] parallel and perpendicular to rows and relaxation of the interlayer spacing. Subsequent annealing at 300 K does not affect the lattice parameters (as denoted by full circles).

note angles for undistorted fcc(311) and bcc(211) arrangements. It is seen that the transformation predominantly takes place in the regime below 5 ML, whereas a residual shear distortion of the bcc(211) arrangement persists for higher coverages.

Apart from the shear distortion, the structural transformation is accompanied by lateral compressions and a vertical expansion of the lattice. This is shown in the lower panel of Fig. 9. In this representation, the lattice parameters are expressed by strains with respect to the bcc(211) equilibrium configuration. Arrows denote lattice parameters expected for pseudomorphism. The lateral lattice parameters derived from integral-order spot positions in the diffraction pattern relate to the lateral spacing between close-packed-atom rows and the nearest-neighbor distance within a row. The mean vertical lattice constant (i.e., the mean step height d of the growth front) is derived by measuring the electron energies for which in-phase scattering is fulfilled. To ensure a correct determination of absolute-energy quantities, the electron gun was calibrated with the help of the XP spectrum of the bare Cu substrate. Due to the obvious roughness of the Fe overgrowth, the determination can be done with high accuracy, since a slight deviation from the condition of constructive scattering between adjacent terraces produces a considerable broadening of the spot profile (compare Fig. 5). In fact, all lattice parameters extracted here are averaged over all layers which contribute to the growth front. Nevertheless, they are a

reliable qualitative measure for the coverage-dependent evolution of lattice distortions. It is important to note that only surface geometries are accessible by LEED. Consequently, the data in Fig. 9 correspond to the lattice parameters in the top layer of the film. Hence, for a proper interpretation the morphology has to be taken into account when conclusions are drawn on the distortion of the entire film.

First, we address the range up to a coverage of 5 ML, where coalescence is completed. In this regime the relaxation of single islands is observed. As a general trend, the lattice parameters (including the shear) relax towards the equilibrium configuration of bcc Fe. Consequently, for 5-ML coverage, the crystallographic arrangement may be interpreted as a highly strained bcc structure. In this case, the residual lattice distortion would result in tensile lateral strains of +4.0% perpendicular and +1.5% parallel to rows, and a compressive vertical strain of about -6% . The presence of a vertical compression corresponds to the expected response to tensile lateral strain. However, the magnitude of vertical strain exceeds considerably the compression expected for a purely elastic response. The latter can be estimated by minimization of the free energy of the strained film.³⁵ Taking the observed quantities for the lateral tensile strains and the shear for a 5-ML-thick film as plotted in Fig. 9, an elastic vertical compression of -2% is calculated. In contrast, the measured vertical strain is larger by a factor of 3. The apparent discrepancy shows that a description on the basis of the elastic properties of intrinsic bcc Fe is inadequate for this highly strained overlayer.

Evaluation of the diffraction data showed that the topography of the growth front remains unchanged for coverages above 5 ML. This is evident from the fixed periodic correlation of the faceted film surface and the constancy of the asperity height Δ (compare Fig. 6). Furthermore, the residual mean surface distortion (as deduced from the observed lattice parameters averaged over the growth front) remains unchanged after coalescence is completed. The resulting surface geometry clearly deviates from a fully relaxed bcc arrangement. This is especially apparent from the residual shear inferred from the upper panel of Fig. 9: the angle between the unit vectors of the surface unit cell remains 83° , while it would measure 90° for undistorted bcc Fe. This observation suggests that a considerable lattice distortion (with respect to bcc structure) persists in the coalesced film which imposes residual shear and strain on the faceted film surface. Consequently, effective rearrangement of close-packed atom rows towards bcc structure only takes place before coalescence is completed (i.e., in single Fe islands) or in the faceted top layer of the coalesced film.

Finally, it is noted that there is a considerable difference in the observed relaxation behavior of the lateral surface strain parallel and perpendicular to close-packed atom rows. The row spacing remains roughly constant over the entire coverage range investigated and measures 4.21 \AA . This value is close to the row spacing of the Cu(311) substrate (i.e., 4.23 \AA). In contrast, the nearest-neighbor distance within rows initially measures 2.55 \AA (which equals the pseudomorphic value) and rapidly decreases with proceeding coverage. This behavior is in accordance with conclusions drawn above: the growth process of the distorted Fe overlayer is driven by the constraint to lower dominant stress along the direction of

uniaxially aligned close-packed-atom rows. This leads to a periodically faceted growth front that promotes effective rearrangement of the lattice along the row direction. On the other hand, the energy cost to dislocate the lattice perpendicular to the rows is likely to be considerably higher, i.e., the bcc overlayer is pinned to the row separation of the template. In fact, such a pinned state is expected to be unstable against the formation of dislocations, since increasing stress accumulates perpendicular to rows while the film grows thicker. Nevertheless, no indication of dislocation-induced strain relief along this direction was found for coverages up to 20 ML.

IV. SUMMARY AND CONCLUSIONS

The structural analysis discussed above gives detailed insight into the coverage-dependent evolution of the structural film properties. In the initial stage of growth, a pseudomorphic Fe overlayer forms on the Cu(311) substrate. Resulting pseudomorphic strain produces dominant stress along the uniaxially arranged close-packed-atom rows which hampers the formation of a compact adlayer. Instead, the attempt to lower stress energy forces the formation of a regular array of fcc Fe patches with a quasiperiodic separation of 35 \AA along the row direction. With proceeding growth, these pseudomorphic patches act as nucleation sites: islands with a periodic separation start to grow and thereby produce a faceted growth front. The relief of uniaxial stress proves to be the driving force for the periodic faceting of the overlayer. For coverages below the completion of coalescence at 5 ML, the crystal structure gradually changes to a (211)-oriented strained bcc-like arrangement via a Pitsch transformation. As a remarkable result, this gradual transition represents a significantly different scenario compared to the well established structural transformation in Fe films on Cu(100).⁷⁻¹⁰ In the latter case a martensitic, i.e., a sudden and collective transition to fully relaxed bcc structure occurs at ~ 10 -ML coverage, which is accompanied by a dramatic change of the film morphology. Here, a continuous relaxation of the lattice distortions is observed in the initial stage of growth. The spatial anisotropy, that is, the surface topography of a regular up-and-down staircase along the row direction is preserved over the entire coverage range investigated. We attribute this different behavior to the following. First, the shear distortion and the lattice compressions and expansions necessary to transform the Fe overlayer from (311)-oriented fcc to (211)-oriented bcc structure are considerably smaller compared to those present in the case of (110)-oriented bcc Fe films on Cu(100). Most important, however, the formation of separate 3D islands for coverages below 5 ML [in contrast to layer-by-layer growth for Fe/Cu(100)] leads to effective relaxation toward a strained bcc structure. The latter conclusion is supported by the observation that the relief of shear and strain in the top layers of the film terminates at 5-ML coverage, where coalescence is completed. The coalesced film, on the other hand, locks into a lattice arrangement that is likely to be predominantly dictated by the substrate surface corrugation and thus should correspond to a fcc-like structure. This is apparent from residual shear and strain in the faceted film surface which is imposed by the coalesced film and remains unchanged with proceeding coverage. A precise

quantification of the lattice arrangement within the coalesced film is difficult on the basis of our data, since LEED detects surface geometries only. Nevertheless, following the above line of reasoning we can draw conclusions about the qualitative evolution of the lattice distortions: effective rearrangement towards bcc structure only takes place before coalescence is completed (i.e., for coverages <5 ML) and in the faceted top layers of the coalesced film. In summary, the structural properties of ultrathin Fe films on Cu(311) turn out

to be ruled by an intimate interrelationship between morphological features and lattice distortions of the overlayer.

ACKNOWLEDGMENTS

We thank J. Wollschläger, M. Horn-von Hoegen, and R. Koch for helpful discussions. Partial support of this work by the Deutsche Forschungsgemeinschaft, Sonderforschungsbereich 290, is gratefully acknowledged.

-
- ¹S. H. Lu, J. Quinn, D. Tian, F. Jona, and P. M. Marcus, *Surf. Sci.* **209**, 364 (1989).
- ²H. Landskorn, G. Schmidt, K. Heinz, K. Müller, C. Stuhlmann, U. Beckers, M. Wuttig, and H. Ibach, *Surf. Sci.* **256**, 155 (1991).
- ³P. Bayer, S. Müller, P. Schmailzl, and K. Heinz, *Phys. Rev. B* **48**, 17 611 (1993).
- ⁴M. Wuttig and J. Thomassen, *Surf. Sci.* **282**, 237 (1993).
- ⁵N. Memmel and T. Detzel, *Surf. Sci.* **307-309**, 490 (1994).
- ⁶S. Müller, P. Bayer, C. Reischl, K. Heinz, B. Feldmann, H. Zillgen, and M. Wuttig, *Phys. Rev. Lett.* **74**, 765 (1995).
- ⁷M. Wuttig, B. Feldmann, J. Thomassen, F. May, H. Zillgen, A. Brodde, H. Hannemann, and H. Neddermeyer, *Surf. Sci.* **291**, 14 (1993).
- ⁸K. Kalki, D. D. Chambliss, K. E. Johnson, R. J. Wilson, and S. Chiang, *Phys. Rev. B* **48**, 18 344 (1993).
- ⁹J. Giergiel, J. Kirschner, J. Landgraf, J. Shen, and J. Woltersdorf, *Surf. Sci.* **310**, 1 (1994).
- ¹⁰P. Schmailzl, K. Schmidt, P. Bayer, R. Döll, and K. Heinz, *Surf. Sci.* **312**, 73 (1994).
- ¹¹V. L. Moruzzi, P. M. Marcus, and J. Kübler, *Phys. Rev. B* **39**, 6957 (1989).
- ¹²D. Li, M. Freitag, J. Pearson, Z. Q. Qui, and S. D. Bader, *Phys. Rev. Lett.* **72**, 3112 (1994).
- ¹³U. Gradmann, in *Handbook of Magnetic Materials*, edited by K. H. J. Buschow (Elsevier, Amsterdam, 1993), Vol. 7, p. 1.
- ¹⁴B. Schulz and K. Baberschke, *Phys. Rev. B* **50**, 13 467 (1994).
- ¹⁵M. R. Mruzik and G. M. Pound, *J. Phys. F* **11**, 1403 (1981).
- ¹⁶U. Scheithauer, G. Meyer, and M. Henzler, *Surf. Sci.* **178**, 441 (1986).
- ¹⁷J. Wollschläger, J. Falta, and M. Henzler, *Appl. Phys. A* **50**, 57 (1990).
- ¹⁸D. A. Steigerwald, I. Jakob, and W. F. Egelhoff, Jr., *Surf. Sci.* **202**, 472 (1988).
- ¹⁹M. Horn-von Hoegen, T. Schmidt, G. Meyer, D. Winau, and K. H. Rieder, *Phys. Rev. B* **52**, 10 764 (1995).
- ²⁰J. Tersoff and R. M. Tromp, *Phys. Rev. Lett.* **70**, 2782 (1993).
- ²¹O. L. Alerhand, D. Vanderbilt, R. D. Maede, and J. D. Joannopoulos, *Phys. Rev. Lett.* **61**, 1973 (1988).
- ²²D. Vanderbilt, *Surf. Sci.* **268**, L300 (1992).
- ²³D. Vanderbilt, O. L. Alerhand, R. D. Maede, and J. D. Joannopoulos, *J. Vac. Sci. Technol. B* **7**, 1013 (1989).
- ²⁴K. Kern, H. Niehus, Z. Schatz, P. Zeppenfeld, J. Goerge, and G. Comsa, *Phys. Rev. Lett.* **67**, 855 (1991).
- ²⁵F. K. Men, W. E. Packard, and M. B. Webb, *Phys. Rev. Lett.* **61**, 2469 (1988).
- ²⁶P. Zeppenfeld, M. Krzyzowski, C. Romainczyk, G. Comsa, and M. G. Lagally, *Phys. Rev. Lett.* **72**, 2737 (1994).
- ²⁷P. Hahn, J. Clabes, and M. Henzler, *J. Appl. Phys.* **51**, 2079 (1980).
- ²⁸M. Albrecht, H. Fritzsche, and U. Gradmann, *Surf. Sci.* **294**, 1 (1993).
- ²⁹C. Jensen, K. Reshöft, and U. Köhler, *Appl. Phys. A* **62**, 217 (1996).
- ³⁰M. Horn-von Hoegen, A. Al Falou, B. H. Müller, U. Köhler, L. Andersohn, B. Dahlmeier, and M. Henzler, *Phys. Rev. B* **49**, 2637 (1994).
- ³¹M. Horn, U. Gotter, and M. Henzler, *J. Vac. Sci. Technol. B* **6**, 727 (1988).
- ³²M. Henzler, in *Festkörperprobleme XIV*, edited by J. Treusch (Vieweg, Braunschweig, 1979), p. 185.
- ³³M. Albrecht, U. Gradmann, T. Reinert, and L. Fritzsche, *Solid State Commun.* **78**, 671 (1991).
- ³⁴M. Henzler, in *Electron Spectroscopy for Surface Analysis*, edited by H. Ibach (Springer, Berlin, 1977), p. 117; M. Henzler, in *The Structure of Surfaces*, edited by M. van Hove and S. Y. Tong, Springer Series in Surface Science Vol. 2 (Springer, Berlin, 1985), p. 351.
- ³⁵F. Jona and P. M. Marcus, *Crit. Rev. Surf. Chem.* **4**, 189 (1994).